NASA CR-
160316

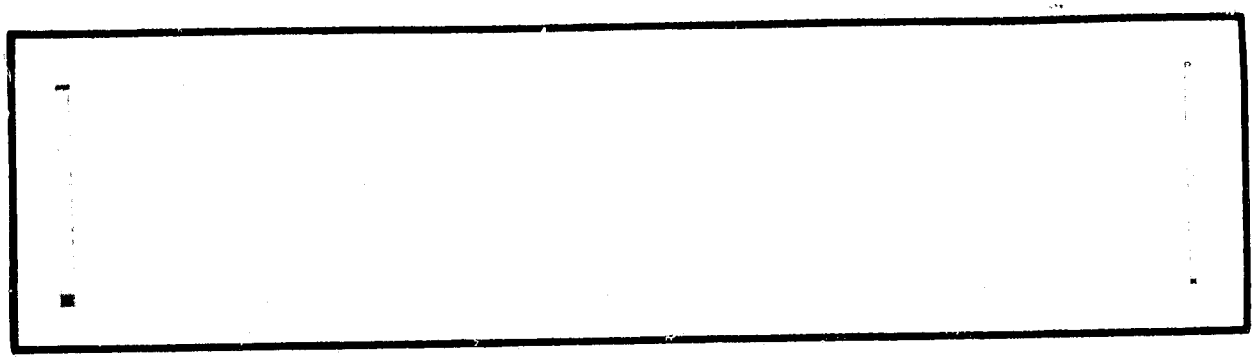

Axiomatix

(NASA-CR-160316) SHUTTLE ORBITER KU-BAND RADAR/COMMUNICATIONS SYSTEM DESIGN EVALUATION: HIGH GAIN ANTENNA/WIDEBEAM HORN Interim Report (Axiomatix, Los Angeles, Calif.) 52 p HC A04/MF A01 CSCL 22B G3/16

N80-10275

Unclas 45855

SHUTTLE ORBITER KU-BAND RADAR/COMMUNICATIONS SYSTEM DESIGN EVALUATION

HIGH GAIN ANTENNA/WIDEBEAM HORN

Contract No. NAS 9-15795

Task #1 Interim Report

(JSC Technical Monitor: E. B. Walters)

Prepared for

NASA Lyndon B. Johnson Space Center
Houston, Texas 77058

Prepared by

R. Iwasaki
J. Dodds
P. Broad

Axiomatix
9841 Airport Blvd., Suite 912
Los Angeles, California 90045

Axiomatix Report No. R7908-5
August 31, 1979

TABLE OF CONTENTS

LIST OF FIGURES

1.0 INTRODUCTION/BACKGROUND

Axiomatix has been tasked by NASA JSC to evaluate the design of the Shuttle Ku-band high gain antenna and widebeam horn antenna. This is Task #1 of contract NAS 9-15795. The high gain antenna is used both for rendezvous radar and communications. In the radar mode, the antenna is linearly polarized, and in the communication mode it is circularly polarized. The widebeam horn antenna is to be used for sidelobe discrimination in the radar mode and as a TDRS acquisition aid in the communications mode.

In this report we describe the antenna suit, with emphasis on the design aspects which produce performance degradation. Design changes are suggested to improve the antenna system performance. In addition to the electrical (RF) problems being encountered, mechanical resonances in the antenna structure as well as excessive drifts, possibly due to servo components and gyros, have seriously impaired the scan performance of the antenna, particularly in the radar mode. The resonance and drift problems are currently under active investigation by Rockwell, HAC and Axiomatix. Results and recommendations in this area will be covered in a subsequent report; however, in anticipation of continued scan difficulties, the radar detection performance as a function of scan overlap has been analyzed and is included in Appendix A.

A primary area of concern in the performance of the high gain antenna is the higher than expected sidelobe levels. In the communications mode (circular polarization) a sidelobe level of -20.6 dB has been measured in the azimuth plane. This is close to the expected variation of the received TDRS forward link signal, and acquisition with a sidelobe cannot be precluded.

If the sidelobes cannot be reduced to acceptable levels, an alternate technique must be used to reduce the possibility of sidelobe acquisitions. Candidate schemes include tighter power control of TDRS, reduced receiver sensitivity, or multiple detection thresholds.

In the radar mode (linear polarization) a sidelobe level of -16.8 dB in the azimuth plane has been measured. The radar sidelobe avoidance technique uses the widebeam horn to discriminate a sidelobe from the peak of the high gain antenna. It is anticipated that the horn will be circularly polarized to optimize communication performance, and hence a 3 dB degradation will be experienced in the radar mode. However, if the proper technique is used for

radar sidelobe avoidance, e.g., relative comparison of the received power in the high gain antenna and the horn, there appears to be adequate margin.

In order to improve the sidelobe levels of the high gain antenna, Hughes has experimented with several types of feeds. Axiomatix, in this report, suggests other passive changes to improve the sidelobe levels.

The impact of maintaining linear polarization with the widebeam horn on TDRS acquisition is examined, as is the impact of circular polarization on radar sidelobe avoidance. With linear polarization, the Shuttle cannot meet EIRP specification in the communication mode, which means that TDRS must open loop point the KSA antenna accurately enough to ensure that adequate power is received at the Shuttle for a successful scan.

2.0 SUMMARY

In section 3.0 we describe the physical characteristics of the high gain antenna reflector and feed elements. Deficiencies in the sum feed are discussed, and lack of atmospheric venting is posed as a potential problem area. In section 4.0, we discuss the measured RF performance of the high gain antenna and relate the high sidelobe levels measured to the physical characteristics of the antenna.

Concern has been expressed as to temperature effects on the performance of the high gain antenna. In section 5.0, we discuss attributes of the feed which might be influenced by temperature extremes, and conclude that the antenna should be insensitive to temperature variations.

In section 6.0, we give detailed suggestions for improvements to the high gain antenna system. In particular, the feed support bipod structure is considered a significant contributor to the high sidelobe levels measured in the azimuth plane. Pod relocation, material changes, and shaping are suggested as improvements. Alternate feed designs are presented to further improve system performance. The exact degree of improvement will be difficult to estimate analytically; it is suggested that these changes be implemented experimentally and the effects measured.

Section 7.0 contains a description of the widebeam horn, with a discussion of potential temperature effects due to the polarizer. In Section 8.0, we discuss the effects of linear polarization on TDRS acquisition, and the effects of circular polarization on radar sidelobe avoidance.

Appendix A presents an analysis of the radar detection probability as a function of scan overlap and target range.

3.0 GENERAL DESCRIPTION, HIGH GAIN ANTENNA

The Ku-band high gain antenna system is a prime focus paraboloid with linear polarization for the rendezvous radar function and right-hand circular polarization for the communications mode. A monopulse comparator subsystem is included to maintain tracking capabilities during operational use. The antenna system is stowed in the Orbiter payload bay during launch and reentry and is only deployed on orbit for rendezvous and communications in space.

Because of the tight stowage requirement, the focal length f(10 inch) of the paraboloid had to be substantially decreased to fit within the volume allotted. The diameter of the dish itself (36 inches) was maintained to be as large as deemed feasible to achieve the narrow 3 dB beamwidths (1.6°) desired. Therefore, the subsequent f/D ratio, a design parameter of reflector antenna systems, was extremely low (0.28), and this greatly affected the overall antenna performance from that predicted by Hughes during the Conceptual Design Review.

In order to reduce the weight of the deployed antenna system, a lightweight graphite epoxy paraboloid antenna was employed. This reflector is composed of layers of woven carbon fiber cloth impregnated with epoxy formed on a master mandrel to mold it to the appropriate contours. Stiffening structures, also made of graphite epoxy, are then bonded at the rear of the reflector to add strength and reduce inertial flexing of the surface. The reflector surface itself is not metallized, depending on both the anisotropic conductivity and the dielectric mismatch of the epoxy/free space interface for high reflectivity.

The feed for the antenna system is composed of a sum horn and monopulse tracking elements, the combination of which create a parasitic mutual coupling effect which appears to degrade the system performance. In order to describe the feed system, however, the two subsystems will be described separately.

3.1 Antenna Sum Feed

The sum feed is composed of a short section of square waveguide that gradually tapers into the circular waveguide feed aperture which is 0.5 inch in diameter. Since the physical dimensions of the aperture

were reduced to permit the placement of the surrounding monopulse elements, the sum feed aperture is filled with a shaped teflon plug to increase the effective circular waveguide diameter sufficient to sustain the proper propagating modes.

The placement of the orthogonal coaxial probe feeds which create the circular polarization capability was experimentally determined by actual measurements. Theoretically, the optimum placement of the probes is a quarter of the guide wavelength in front of the short, which is the position of maximum electric field. Due to the tight space restrictions, the orthogonal wire short of the probe closest to the aperture was placed closer than desirable to the second probe, which can adversely affect the cross polarization isolation. Earlier, coplanar orthogonal probes were attempted, but due to mutual coupling effects, this approach was discontinued.

The lengths of the center coaxial probes extending into the waveguide were also experimentally determined by adjusting the length of a variable center conductor probe into a matched load terminated waveguide and measuring the return loss. This design approach generally is valid, except that for short waveguide sections with multiple discontinuities, the final overall matching must be accomplished after the total feed, including the monopulse elements, are assembled. Since the voltage standing wave ratio (VSWR), a measure of the impedance mismatch, was subsequently reduced from 1.5 to 1.2 or less during the latter phases of testing, it is assumed this latter procedure was performed.

The actual sum feed aperture extends 0.1 inch past the two inch square ground plane. This circular "lip" provides some reduction in the mutual coupling effects between sum feed and the adjacent monopulse elements. The inserted teflon plug, which is physically captured within the circular waveguide when the back half of the feed section is attached, completely fills the waveguide. The tapered aperture end is about 0.3 inch long. The opposite end is counterbored to facilitate the transition to the square waveguide. Various dielectric rod antenna shapes were extended out from the radiating circular aperture, but because of the mutual coupling effects with the monopulse elements and the related high sidelobe levels, a tapered teflon plug that did not extend past the circular waveguide lip was finally chosen. It appears that this lip aids in the launching of the radiated wave; however, some diffraction effects are still obviously present. The height of this

lip was experimentally determined to minimize the sidelobe level, which increased substantially after incorporation of the monopulse elements around the sum feed. It appears that little more could be done to increase this isolation, such as corrugations or chokes, since the monopulse elements are located immediately adjacent (in fact are bent around) the sum feed. One possible modification to reduce this mutual coupling is included in Section 6.0, which lists recommendations for improvement.

No impedance transition provisions (such as a tapered horn) into free space were included in the design. In fact the best description of the radiating aperture would be a rather abrupt dielectric/free space interface at the end of a circular waveguide. Therefore, it is questionable whether a spherical wavefront is radiated from this open-ended waveguide sum feed. The concept of generating a plane wavefront from a paraboloid relies on a spherical wavefront emanating from the prime focus; therefore, some of the inherent degradation in expected low sidelobe levels can be attributed to the sum feed design. Another area of concern is the illumination at the edges of the reflector dish is partially blocked by the side support pods, which greatly distorts the illumination taper.

An earlier version of this antenna system used a four inch square ground plane housing the monopulse phase comparator in conjunction with the feed. Obviously this constituted too much blockage of the antenna system and significant improvements in sidelobe levels were noted when the ground plane cross-section was reduced to a two inch square feed and the large comparator was relocated along the feed support.

3.2 Antenna Monopulse Elements

The monopulse elements consists of four short waveguide sections terminated into receiving slots which detect comparative phase differences between opposite pairs of elements, thereby indicating the proper direction the antenna must be pointed to perform the tracking function. Again coaxial probes are used as transducers to transfer the signals in the waveguide to the semirigid coaxial cables which go to the comparator circuit located on the feed mount. The placement and lengths of the coaxial probes, as well as the dimensions of the slots, were experimentally derived by radiating into a matched load or free space and minimizing the VSWR. The length of the short waveguide sections was determined by the allotted feed envelope, and no resonance effects were utilized in the overall design. The basic

feed performance was determined to be essentially frequency independent within the frequency range of interest. Therefore, it is also relatively temperature independent. (A more detailed discussion of the thermal effects will be made in a later section which will delve into the large temperature extremes to be encountered).

A number of different types of monopulse elements were tested. A standard monopulse system successfully employed on other programs consisted of printed circuit dipoles and, therefore, these elements were initially used. Various geometric configurations such as "in-line" and "star" lay outs were tried, but the final monopulse system utilizes slots in a ground plane forming a small planar array surrounding the sum feed. The reasons that this particular design was selected were that its performance was comparable to the other configurations, fabrication was simpler and dimensional reproducibility was better. The presence of the dipoles protruding above the ground plane also increased the amount of coupling of the sum feed to the monopulse elements.

The feed is machined out of a block of aluminum which is then gold-plated to reduce resistive losses and minimize the effects of corrosion. The feed consists of two halves which are bolted together. The front half consists of the circular sum feed and the slotted waveguides of the monopulse elements. The rear half contains the sum feed square waveguide and the coaxial probe connections. Since intricate machining is required, electron discharge machining (EDM) is extensively used to form precise corners.

A front and cross-sectional views of the sum feed and monopulse elements are sketched in Figure 1 to illustrate the design. Figure 2 shows the overall feed and support structure with the attached monopulse comparator circuitry. It can be seen that the feed does cause significant blockage in the crucial central portion of the dish, even after the reduction of the feed cross-section by relocating the phase comparator circuitry.

3.3 Additional Feed Design Considerations

One aspect of the design that has not been discussed but must not be overlooked is to incorporate adequate venting provisions to prevent damage to the protective 5 mil kapton windows over the monopulse

elements and the inserted teflon plug of the sum feed due to the abrupt pressure changes arising from launch. The large pressure differentials can cause separation of the windows or loss of the teflon plug, the latter effect being critical since the sum feed cannot propagate Ku-band microwave signals without the dielectric medium in the reduced diameter circular waveguide. Even if only partial ejection of the teflon plug occurred, the resultant protrusion would behave like a dielectric rod antenna with the earlier observed effect of parasitic coupling to the monopulse elements and therefore result in much higher sidelobe levels.

Vents can be introduced in a number of positions without greatly affecting the RF performance. For example, since the feed is a two piece flanged section, small holes can be machined at the flange face in the corners of all five waveguides since the electric fields are negligible there. Similarly, small holes can be drilled at the corners of the rear walls of the waveguides at the plane of the short but this is more difficult to align. Since the semirigid coaxial cable probe is usually filled with a dielectric (teflon) and the signal strength is greatest there by design, it is probably wise to avoid these areas for venting purposes.

Hughes has subjected a breadboard feed design to an abrupt vacuum test, with no adverse effects. It was felt that adequate venting was provided by the nonhermetic seal connector probes and loose fitting flanges. The test involved decreasing the pressure from atmospheric to 10^{-3}mm (Hg) of vacuum in about 15 seconds. Although it appears adequate, more details of the exact launch profile depressurization should be known. And prudent design would incorporate venting provisions to accommodate multiple launches.

Another concern is the effect of ultraviolet light from the sun affecting the material properties of the teflon plug in the sum feed which is critical to the proper operation of the radar and communication modes. Although in the low f/D ratio antenna system the feed is blocked effectively from direct exposure to the sun, whatever energy that is reflected from the reflector is highly concentrated since it is focussed at the feed. A protective kapton window might also be considered to cover the sum feed aperture, similar to the kapton windows used for the monopulse elements.

4.0 RF PERFORMANCE

The RF performance of the Ku-band antenna system reflects the fact that a low f/D ratio prime focus system was selected over a larger f/D ratio system such as a Cassegrain with a subreflector. The higher than expected sidelobe levels, which may result in inadvertent sidelobe acquisition, arises from two separate effects. First, the center-fed parabola has a large amount of blockage from the feed, feed support, and pods. Second, the sum feed system, composed of a dielectric loaded circular waveguide, is not noted for its illumination taper or its spherical wavefronts, and parasitic mutual coupling to the monopulse elements is evident. It is essential to characterize the apparent causes of these limitations so that future modifications, if required, will be straightforward.

The measured principal plane antenna patterns are shown in Figure 3 and 4 for two typical modes: linear polarization and circular polarization at 13.77 GHz. Examining these patterns reveals some basic characteristics which will generally suffice to describe the pattern at other frequencies, since it was designed to be a wideband system. As depicted in the circular polarization case pattern of Figure 3, the elevation plane (denoted by EL) possibly shows the blockage effects of the feed support by the lower than -30 dB sidelobe. Generally this obstructed energy is simply redistributed, and it is not uncommon to find sidelobes in another region greater than would be measured if the blockage did not exist, due to the disturbance in the interference patterns. Although a raster scan was made of the immediate vicinity of the main beam, a more thorough program of antenna pattern measurements should be conducted for the final flight version to verify that no extraneous sidelobes of substantial magnitude exist.

The measured 3 dB beamwidth is broader than originally specified (1.5°-1.6°) but the increase does not appear to be significant. The measurement techniques used the expanded scale (6x magnification) to resolve the angular relationship to greater than tenths of a degree, and calibration curves of the pattern measurement system were taken at a later date to confirm that nonlinearities did not exist. In practice, especially when the flight model antenna patterns are measured, calibration verification curves using a series-connected precision attenuator might be recorded both before and after a series of patterns to conclusively demonstrate the validity of the beamwidth and sidelobe levels.

The -16.8 dB sidelobes in the azimuth plane are unreasonable. Although this behavior is attributed to a nonideal ADL paraboloid reflector, there may be some other suitable explanations. One possibility, which will be discussed further in the last section which deals with recommended improvements, addresses the placement of the graphite epoxy feed supporting pods which are in the azimuth plane and block the illumination taper. Another is the existence of parasitic mutual coupling of the sum feed with the monopulse elements since the primary sum feed radiation pattern is greatly distorted when the monopulse elements are added.

5.0 THERMAL EFFECTS ON THE Ku-BAND FEED

The calculated temperature extreme that the Ku-band feed will be subjected to is approximately -170°F (160°K). Therefore, some concern has been expressed as to the temperature dependence, if any, of the feed. Attempting to utilize the existing knowledge of the present design, especially the measured wideband frequency performance, it does not appear that there are any critical temperature-dependent effects which might adversely affect the feed performance, excluding possible mechanical stresses and material phase transitions. The design parameters were rather loose; many aspects of the design were experimentally determined and, therefore, not subject to precise dimensions. As a result, thermal expansion and contraction effects were, therefore, minimized for this wideband system. No sensitive resonant cavities or filters which might be detuned by thermal dimensional changes were incorporated into the design. The closest structures that resemble a resonant cavity are the short waveguide sections of the monopulse elements with the radiating slots. Experimentally, however, these elements have been measured to operate over the range 13.75 to 15.15 GHz and therefore do not seem temperature-sensitive since they are not frequency-sensitive.

Under standard laboratory conditions, it is very difficult and expensive to measure the performance of an antenna system over the anticipated operating temperatures of space since the feed would have to be cryogenically cooled below the dew point of the surroundings, necessitating enclosure within a vacuum chamber. Further, the essential antenna parameters, beamwidth and sidelobe level measurements require far field pattern measurements, so that a large transparent vacuum chamber window would be required. Thus, the temperature dependence measurements of an antenna system would have to be considered impractical on the ground. The best one could realistically achieve is, possibly, to measure the return loss of a cooled and heated feed assembly in a vacuum chamber with the feed pointed at a matched load. Swept frequency measurement could then establish whether temperature-dependent effects exist.

In response to the concern shown over the temperature dependence, a simple heating test of the feed was made using a heat gun during antenna pattern measurements. As would be expected, no effects were noted. It is felt that such tests are not truly representative since the feed will

assume a very low temperature, and the temperature differential calculated will be much larger than can be achieved under these conditions.

Rather than speculate on the effects of the calculated cold temperatures, it might be more productive to examine potential solutions to the problem. The present thoughts involve adding a strip heater to the feed assembly, similar to that used to warm the monopulse comparator circuitry. Rather than using active heating, however, if passive means are available for thermal control, then these methods should be looked at instead of wasting valuable electrical power. A thermal enclosure about the feed and feed support would greatly reduce the temperature extremes presently expected. This enclosure could be in the wedge shape described later to minimize RF blockage effects. It would also serve to protect the feed, comparator, and connecting cables from physical damage due to deployment and stowage.

6.0 RECOMMENDATIONS FOR IMPROVEMENT

One of the goals of the Ku-band antenna study is to make recommendations, if possible, to improve the performance of the system. After describing the antenna in some detail, some areas of improvement became apparent, especially in regards to the higher than expected sidelobe levels. This section outlines some modifications which seem reasonable to investigate further.

One of the explanations for the poor sidelobe performance of the Ku-band antenna is the mutual coupling effects between the sum feed and the monopulse elements. The primary sum feed antenna pattern is disturbed significantly when the monopulse elements are added. The original 20 dB taper on the reflector is reduced to a 10 dB taper. In order to reduce this mutual coupling, the addition of shorting elements on the ground plane to place the null from the VSWR on the monopulse slots is proposed. Earlier Hughes tests of a similar technique indicated substantial perturbations in pattern measurements by the placement of obstacles on the ground plane, but efforts were discontinued due to the poor results. In the next section we describe a more systematic technique for the placement of shorting elements.

The other major contributor to high sidelobe levels appears to arise from the blockage of the primary sum feed illumination pattern by the adjacent feed support pods in the azimuth plane. Three modifications are suggested. The first is to relocate the pods out of the azimuth plane preferably into positions 120° from the feed support to disrupt the cumulative blockage of both pods in one plane. If it is determined that actually little mechanical support of the feed is required, then possibly only one support pod parallel to the boresight of the sum feed might be studied. A better solution is to attach the pods at 120° angles to the edge of the reflector such that the pods only block the secondary pattern from the illuminated reflector. The amount of effective blockage for this configuration is much less, even though the pods are longer. And finally, a nonconductive material can be used to fabricate the pods instead of conductive graphite epoxy.

A more subtle design method might also be used to decrease the effective blockage cross-section. Shaping the pods and feed support into diamond and hexagonal wedges can greatly reduce the deleterious effects of the obstacles.

And finally, in order to control the launching of spherical wave fronts by using a dielectric lens concept, some possible design shapes for the dielectric plug are developed.

6.1 Reduction of Mutual Coupling Effects

There was a noticeable degradation in the illumination taper of the primary pattern of the sum feed when the monopulse elements were incorporated. In order to attempt to alter this deleterious interaction, a slight modification of the ground plane is proposed to create an effective short for the leakage radiation diffracted around the lip of the sum feed. This short is positioned to take advantage of the directionality of the leakage radiation compared to the incident radiation from the reflector.

Basically the idea is to position a null from the resultant standing wave from the short at the slot center. As Figure 5 indicates, the location of this annular ring sector is $3/4\lambda$ from the sum feed. The height of the short should be approximately that of the extension of the lip of the sum feed, but the exact dimension would probably be experimentally determined.

The incident radiation from the reflector should not be adversely affected by this annular ring sector short by geometrical considerations since the height is small compared to a wavelength and the separation between the annular rings is greater than $\lambda/2$, which avoids reactive termination conditions as in corrugations.

If improvement is noted, then it would be logical to add other annular ring sectors $\lambda/2$ beyond the first one to improve the effectiveness of the short.

6.2 Pod Relocation

The blockage effect of a center fed paraboloid is especially critical since the majority of the illumination taper of the feed is in the central area of the dish, and therefore any obstruction greatly alters the antenna pattern, usually by broadening the beamwidth and increasing the sidelobe levels.

The most logical explanation for the degraded sidelobe behavior for the linear polarization case (and therefore the circular polarization case is the use of horizontal graphite-epoxy support pods for mechanical rigidity of the main feed support. Since graphite epoxy is considered conductive, these pods have a large effect blockage cross-section, similar to the reason for changing the orientation of linear polarization with respect to the feed support.

A sketch of the physical relationship between the sum feed pods and reflector is shown in Figure 6a. Although the pods are relatively short, they would exert substantial influence on the patterns since they are positioned so that all radiation in that plane is blocked. Since the f/D ratio of the antenna is so low, the effective blockage cross-section is large because the angles subtended by the pods increase when the pods are located closer to the focus. In this particular case, the pods are so close to the center of the paraboloidal reflector that they intrinsically will obstruct the primary pattern of the sum feed even before illuminating the reflector, as depicted in Figure 6b. If the edge of the reflector is roughly ±70° from the sum feed, the pods are approximately ±30° from the center (more exact angular relationships should be obtained if further analysis is desired). Thus the primary pattern of the sum feed is completely blocked in the azimuth plane beyond the 30° from boresight. Further, the central portion of the primary pattern after reflection is blocked by the feed, but this blockage cross-section has been greatly reduced by the relocation of the phase comparator and the reduction of the ground plane area to 4 square inches. Thus the presence of the support pods, being conductive, completely disrupts the primary and secondary patterns, resulting in poor sidelobe levels.

If the support pods were attached to the edge of the reflector instead of the central area, the effective blockage cross-section would be reduced and the sidelobes correspondingly reduced in magnitude, as sketched in Figure 6c.

6.3 Pod Orientation

Conductive support structures are known to affect patterns for the case when the electric field is parallel to the conductive member. The explanation, it appeared, was that the conductive member acted in a manner to electrically short the incident electric fields, creating a standing wave in the vicinity of the parallel member. Electric field vectors orthogonal to the conductive member, however, can propagate around the obstacle since electric fields can exist normal to a conductive surface. For the case of circular polarization, since the electric field vector rotates, the standing wave phenomenon is similarly applicable for the parallel

component of electric field but not for the orthogonal component. Therefore, a polarizing mechanism exists, similar to the wire grid structures used to filter out the orientation of linear polarization parallel to the wires.

This effect was noted early in the development of this Ku-band antenna. The sidelobe levels decreased when the orientation of linear polarization was rotated to the azimuth plane, which is perpendicular to the feed support. However, now the support pods became aligned parallel to the electric field and became predominant blocking mechanism, although to a lesser extent.

If the support pods were located 129° from the feed support, the sidelobes would be further reduced since the blocked areas are not in the same plane. Therefore the magnitude of the perturbation is caused by only one pod, which is not the present situation where there are two pods in the azimuth plane, the plane which has the high sidelobe problem. By distributing the disturbances due to the pod placement about the antenna pattern, it is possible to reduce the sidelobe contributions in any single plane, thereby decreasing the sidelobe level.

6.4 Pod Material

The reason why the side support pods result in such large blockage is the fact that graphite-epoxy is quite conductive and, therefore, creates standing waves patterns in the region of the pods.

One solution is to fabricate the pods from less conductive material such as fiberglass or kevlar. These materials, being dielectrics, would cause some phase shift problems for the rays incident upon the pods, but actual blockage would be minimized.

One potential problem area if material substitution is used is thermal expansion differentials since graphite epoxy is noted for its low coefficient of thermal expansion. For the relatively short pod lengths considered here, however, this should not deter the serious consideration of this approach.

6.5 Pod Shaping

Another approach might be considered to further improve the side-lobe levels. Earlier work by Ruze [1] and Kay [2] discussed the improvement in gain of antennas with blockage of the obstacle was tapered to allow incident radiation to propagate around the obstacle rather than be reflected away by flat surfaces. Their problem was to minimize the effects of metallic structures supporting a radome. On a comparative scale, that type of blockage was very small, since on a cross-sectional basis, the width of the structural members were quite small compared to the antenna reflector cross section. However, for the case of this Ku-band antenna, the feed and feed support structure are quite large compared to the reflector and the microwave wavelengths. Therefore, the shaping of the obstacle should have a correspondingly larger improvement.

The specific shape to be considered is a pyramid over the feed and a hexagonal wedge or a variant thereof along the feed support which will permit some radiation, however distorted, to be collected by the reflector. Ideally, the hexagonal wedge has long tapers on both sides which behave as transitions and provide a grazing incidence angle to the incident radiation. Since the illumination taper is greatest at the center of the dish, the region where the feed is mounted, this area is intrinsically the most critical. An easy test to determine the feasibility of this approach consists of a simple substitution whereby a section of heavy-duty aluminum foil is folded into the appropriate shape and taped onto the breadboard or engineering model. The result should be readily apparent by the measurement of sidelobe levels. This shaped reflector along the feed/feed support can also serve as a thermal shield to reduce the large temperature extremes calculated to exist at the feed. A fiberglass shell bonded with heavy-duty aluminum foil over which is painted with white thermal control point will help to passively maintain the feed at a higher temperature than the

presently calculated -170°F (nonoperational state) and reduce temperature fluctuations on the phase comparator circuitry which have temperature sensitive varactor diodes subject to "carrier freeze-out" at low temperatures.

6.6 Dielectric Plug Design

One design requirement discovered during the early phases of the Hughes antenna feed development was the control of the illumination taper which was too uniform and, therefore, resulted in extremely poor sidelobe levels. After many trial tests, the present dielectric plug shape was evolved which resulted in a satisfactory primary feed pattern without the monopulse elements with a 20 dB taper. (The presence of the monopulse elements, and the mutual coupling, however, reduced it to a 10 dB taper.) This shape is sketched in Figure 7a, which shows a 0.5 inch diameter circular teflon plug tapered at the aperture end to simulate a dielectric rod antenna which concentrates the radiated energy in the dielectric as though it was a dielectric waveguide. The other end of the plug, facing into the coaxial probe transducer, is counterbored to form a transition from the square waveguide to the circular waveguide section. This "concave" surface is conducive to creating a nonplanar wavefront since the central portion of the propagating mode travels at a higher velocity than at the perimeter of the circular waveguide, thereby creating a "bulge" in the wavefront which might result in a quasi-spherical wave at the aperture end since the circular waveguide section is relatively short. However, on the aperture end, the tapered dielectric section used to concentrate the radiated energy acts to slow the central portion of the propagating mode, thereby compensating for the concave surface at the opposite end. A sketch of the probable phase fronts for the present design, which coincides with that actually measured, is shown in Figure 7b. Since the tapered rod was experimentally found to be essential to creating a satisfactory illumination or amplitude taper in the primary pattern, any suggested modifications to improve the antenna performance must realistically use this baseline design.

6.7 Modifications to Promote Spherical Wavefronts

Since collimation from paraboloids rely on a spherical wave emanating from the focus, it would seem logical that an effort would be made to alter the situation to favor creating at least a semblance of such a spherical wave.

This nonspherical wavefront effect would be accentuated for lower f/D antenna systems since a longer focal length geometrically reduces the magnitude of the deviation from a true spherical wave, measured in fractions of a wavelength. The optical equivalent of this situation is spherical aberration, where the degree of distortion corresponds to the sidelobe problem.

A spherical wavefront requires that the central portion of the radiated energy from the feed be launched into free space earlier than that planar wavefront within the dielectric-filled circular waveguide. A sketch of the proposed modifications to the existing teflon plug is illustrated in Figure a. Note that the present design configuration is generally maintained since it has successfully evolved by extensive testing to a satisfactory performance level. Since few further modifications to decouple the sum feed from the monopulse elements are obvious, the spherical wavefronts concept, which has not been emphasized earlier, is pursued.

One method to create this desired effect is to drill a small hole in the center of the teflon plug, thereby creating a propagating mode which can have a longitudinal component of electric field, creating the "bulge" that generates the required curvature at the radiating aperture. Since this perturbation is distributed, the cumulative effect is to cause a high degree of distortion, with the faster central portion of the mode "dragging along" the slower edge portion which serves as a slow wave structure. The depth and diameter of the hole would have to be determined by analysis, but the concept does permit a degree of control over the shaping of the launched wavefront which has not been investigated previously. And, if this hole traverses the entire length of the dielectric plug, it can also serve as a convenient means of venting the square waveguide section of the sum feed to relieve the contained atmospheric pressure during the launch.

Another method of creating a quasi-spherical wave is to shape the dielectric aperture as a lens system. Since a planar propagating wavefront exists within the circular waveguide, the "bulge" can be encouraged by a concave surface, such that the aperture appears indented in the center of the plug. Since the central portion is launched earlier than the edges, a more exaggerated curved wavefront results. Again, further analysis would be required for determining the optimum curvature if the concept is pursued, but a simple experimental verification can be obtained by machining a test teflon plug and comparing the resulting sidelobe levels.

A sketch of the desired phase fronts resulting from these modifications is shown in Figure 8b. Note that although perfect spherical waves are not produced, the general wavefront is not as distorted in terms of the magnitudes of the phase deviations as in Figure 7b.

6.8 Differential Monopulse Element Nulls

The explanation used in Axiomatix Report R7804-3 for the absence of a well-defined null in a particular plane difference channel was attributed to the geometrical relationship of the dipoles to the incoming phase front on which the monopulse tracking system is based. This phase front problem would be more apparent for lower f/D ratios of the antenna reflector systems. The orientation of linear polarization in the plane of incidence suffers from a lack of phase resolution since it approaches the dipole at the grazing angle. Because of this grazing angle of incidence, the phase itself cannot be well characterized by the dipole, which is of the order of half a wavelength long. An attempt to pictorially describe this phenomenon is shown in Figure 9a, which shows that the phase front from the edge of the reflector is incident on the monopulse dipole at close to a grazing angle. A more detailed description is shown in Figure 9b. which shows the phase relationship of the incident wave on the dipole for the ray path designated by A. It is seen that the phase relationship cannot be well defined for this orientation of polarization and this particular dipole orientation. This is not true for the ray path designated B since the electric field vector would be oriented parallel to the dipole, and a prominent null would exist.

One corrective measure would be to use a curved dipole as shown in Figure 9c. This configuration would most closely resemble the focused spherical phase front and would thereby avoid the shallow null problem.

The present monopulse design uses slots in a ground plane, and the same explanation is valid except that now the shallow null is transferred to the orthogonal plane from the case of the dipole. But since the orientation of linear polarization has been rotated to the azimuthal plane, the shallow null is still in the elevation plane. The grazing angle for the slot configuration is shown in Figure 9d, where, due to the finite width of the slot, phase resolution can be degraded for a low f/D system unless a complex spheroidal ground plane is used.

7.0 KU-BAND WIDE BEAM HORN

The Ku-band wide beam horn has two distinct functions. The first use is to determine main beam acquisition for the rendezvous radar by establishing a threshold level for comparison with the narrow beam antenna sidelobes. The second function is the wide area acquisition of the TDRS signal for communications.

Since the TDRS signal is right hand circularly polarized (RHCP) and the radar is linearly polarized, there has been some compromise in the radar performance. There is an inherent 3 dB loss when linear polarization is received with a RHCP horn since the linear polarization is composed equally of right and left hand circular polarization components.

The purpose of this section is to describe the wide beam horn in some detail and determine the system trade-offs. Since the horn was initially designed for linear polarization as a result of a possible Skylab mission, the antenna pattern measurements with the circular polarization transducer are not available at this time. However, the earlier linear polarization measurements indicate reasonable performance parameters.

7.1 Physical Description

The basic conical horn design is a cone with a slope length of 7.7 inches, an aperture diameter of 3.2 inches and a double cone angle of 24°, as sketched in Figure 10. The circular polarization (RHCP) transducer is located immediately behind the horn and consists of a section of circular waveguide with four pairs of tuning screws 45° to the incident linear polarization which act as reactive elements to generate the differential phase shifts required to change the linear polarization to circular polarization.

Some of the general design graphs used to create the differential phase shifts are shown in Figure 11[3] to explain the multiple-lumped-element loading concept of this type of transducer. Instead of a square waveguide, the linear polarization is introduced into the circular waveguide at a 45° angle to simulate a power splitter since the equal orthogonal components parallel and perpendicular to the tuning screws then undergo the differential phase shifts which result in generating circular polarization.

7.2 Pattern Measurements

The only Ku-band wide beam antenna pattern measurements released to datehave been the linear polarization patterns taken for the proposed Skylab mission. Since the wide beam antenna is being converted to right hand circular polarization (RHCP), the patterns themselves can only be used as a representative sample of what might be expected for the RHCP case, although the efficiency of the circular polarization transducer over the broad frequency range will greatly affect the final patterns.

The most noticeable characteristic of this type of conical horn is the varying beamwidths in the E and H planes at the same frequency, as shown in Table 1.

Table 1. Ku-Band Wide Beam Horn-Linear Polarization

Freq. (GHz)	Gain (dB) [at rotary joint]	3 dB Beamwidth (°) - E and H Planes
13.77	18.4	16.6/18.8
13.90	19.0	16.4/19.9
14.00	18.8	16.7/19.0
15.15	19.7	14.4/17.3

This distortion from a "circular" beam causes ellipticity and therefore RHCP polarization loss off-boresight. If the gain magnitude is important, then another horn like the corrugated conical horn which has similar E and H plane beamwidths might be considered as a substitute.

As was mentioned previously for the narrow beam antenna, the inclusion of calibration curves with an in-line precision attenuator both before and after a series of pattern measurements is essential to verify the validity of the beamwidths and gain.

7.3 Design Comments

The smooth conical horn has the disadvantage of greater ellipticity off axis due to the different beamwidths in the E and H planes. Corrugated conical feed horns, on the other hand, are noted for their more equal

beamwidths in both planes, and some thoughts on considering other types of horns might be fruitful.

The use of the multiple-lumped-element loading technique by Hughes for creating circular polarization does optimize the wide bandwidth requirement since the frequencies are 13.775 GHz for the communications receive mode and 15 GHz for the communications transmit mode. It is also easy to design by using lockable tuning screws for final adjustments.

However, because of the existence of tuning screws, there is some frequency dependence for the circular polarizer and therefore certain precautions should be taken. For example, the operation of the circular polarizer should be measured outside the specified frequency range to determine the frequency sensitivity characteristic and thereby deduce the expected temperature sensitivity. Since the tuning screws are located fairly close together and the probe lengths are short, it is not expected that temperature effects would be significant. Again, as in the case of the narrow beam Ku-band feed, it is recommended that passive means of thermal control be employed to protect it against temperature extremes and resulting thermal gradients from the abrupt operation of the transmitter.

8.0 WIDE BEAM HORN PERFORMANCE

Two specific cases of wide beam horn performance are of interest: what is the degradation due to maintaining linear polarization in the communications mode, and what is the effect of going to circular polarization on radar sidelobe discrimination?

With the back up TDRS acquisition mode, the Orbiter radiates a CW signal toward TDRS using the widebeam horn. TDRS acquires and autotracks on this signal, and in turn radiates toward the orbiter, which scans and acquires the TDRS forward link. TDRS requires a minimum of 30 dBW EIRP for autotrack. Present data on the linearly polarized horn indicates a 30 dBW EIRP into a circularly polarized receive antenna over a 10 degree cone, exclusive of polarization losses due to the TDRS Ku-band dish axial ratio ($\leq$1 dB). Up to 0.5 dB additional loss due to the axial ratio may be possible. Specific effects of linear polarization loss due to the TDRS axial ratio depend on the current budget allocation of axial ratio loss between specified antenna gain and polarization loss (0.2 dB, JSC estimate). As this data is made available, a more accurate estimate of the polarization loss due to the linearly polarized horn can be made. In addition, horn performance is specified as 30 dBW EIRP for a 15° cone rather than a 10° cone. Unless the horn performance (gain) can be improved, the additional 3 dB obtained by going to circular polarization will be needed to meet EIRP specifications.

Circular polarization will effect a 3 dB loss in the radar mode with the high gain antenna transmitting linear and the guard (horn) antenna receiving circular polarization. Present data indicates that the relative signal-to-noise ratio with the high gain transmit/receive antenna is 43.8 dB, but for the high gain transmit/horn receive antenna is 21.2 dB, transmitting on the main lobe. In contrast, transmitting with the first sidelobe the high gain transmit/receive SNR is 7.8 dB and high gain transmit/horn receive is 3.2 dB. Using the "main/guard" test, whereby the ratio of the AGC's for the main and guard antennas are compared with a threshold, for a mainlobe hit, the effective AGC ratio is 22.6 dB, while the ratio with a sidelobe hit is 4.6 dB. This should be adequate margin, assuming the full main/guard test is indeed used.

9.0 CONCLUSIONS

The high sidelobe levels of the high gain Ku-band antenna are a primary influence on the antenna system performance. Several relatively easily verifiable improvements have been suggested to decrease the sidelobe levels of the high gain antenna. If effective, these changes may negate the necessity of alternate, more expensive changes to the Shuttle radar/communication system. In particular, specific recommendations have been made to correct the three areas which have been determined to be contributors to the high sidelobe problem. First, the concept of leakage radiation shorting elements on the ground plane was introduced to minimize the parasitic mutual coupling effects between the sum feed and the monopulse elements. Second, the feed support pods have been identified as obstacles in the primary sum feed pattern and therefore pod relocation and shaping and material substitution were suggested as possible remedies to the illumination taper blockage on the reflector. And finally, some ideas on encouraging the launching of quasi-spherical waves from the sum feed were outlined to minimize phase aberrations for the parabolic system.

Circular polarization for the widebeam horn appears to be the appropriate choice. The degradation in radar sidelobe avoidance is not critical, while linear polarization will affect TDRS acquisition performance.

REFERENCES

1. John Ruze. "Feed Support Blockage Loss in Parabolic Antennas," The Microwave Journal, Vol. 11, No. 12, December 1968, pp. 76-80.

2. Alan F. Kay. "Electrical Design of Metal Space Frame Radomes, " IEEE Transactions on Antennas and Propagation, AP-13, No. 2, March 1965, pp. 188-202.

3. H. Jasik, Antenna Engineering Handbook. McGraw Hill, 1961, pps. 17-18, 17-19.

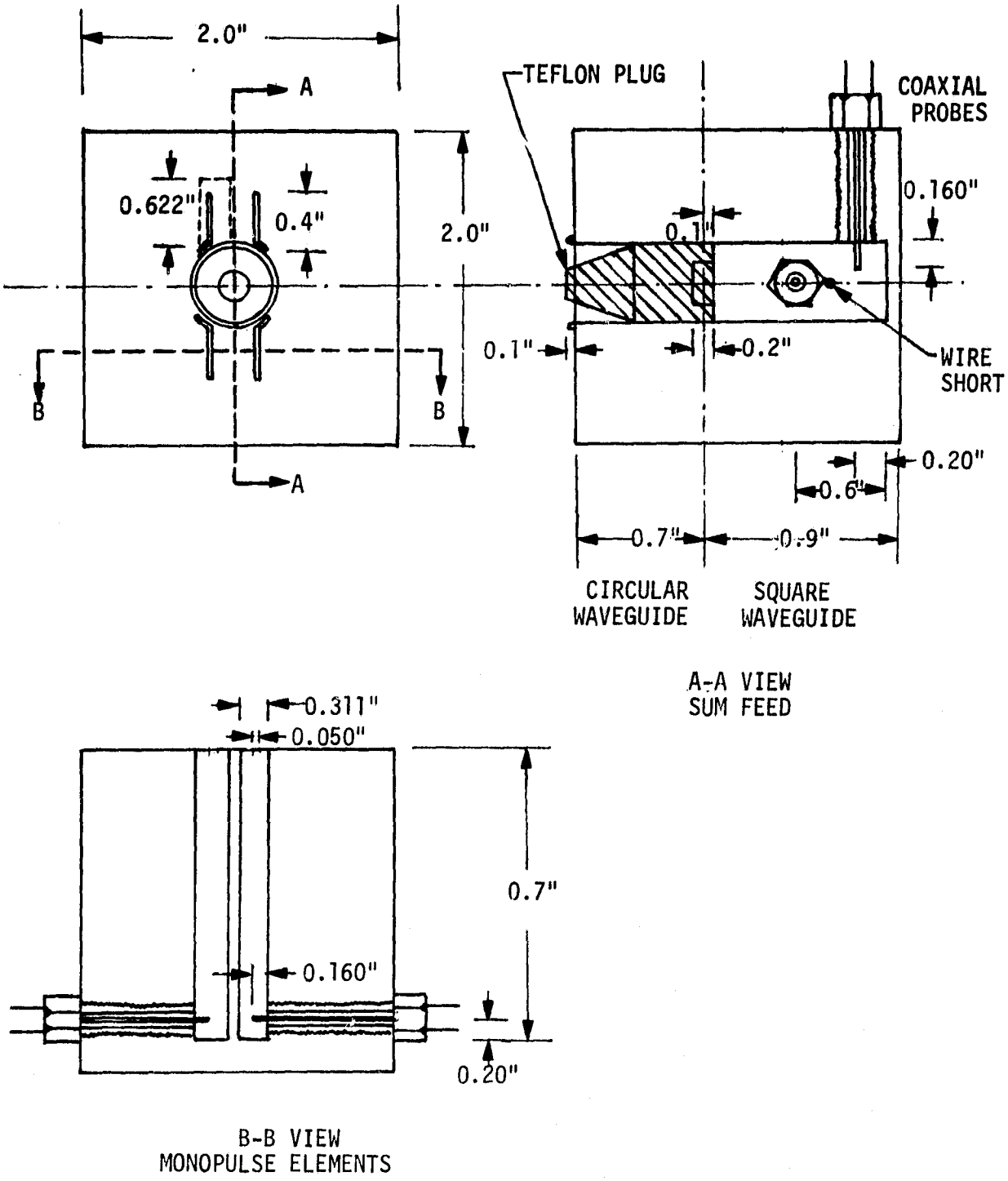

Figure 1. Ku-Band Feed Design Sketch
(not to scale)

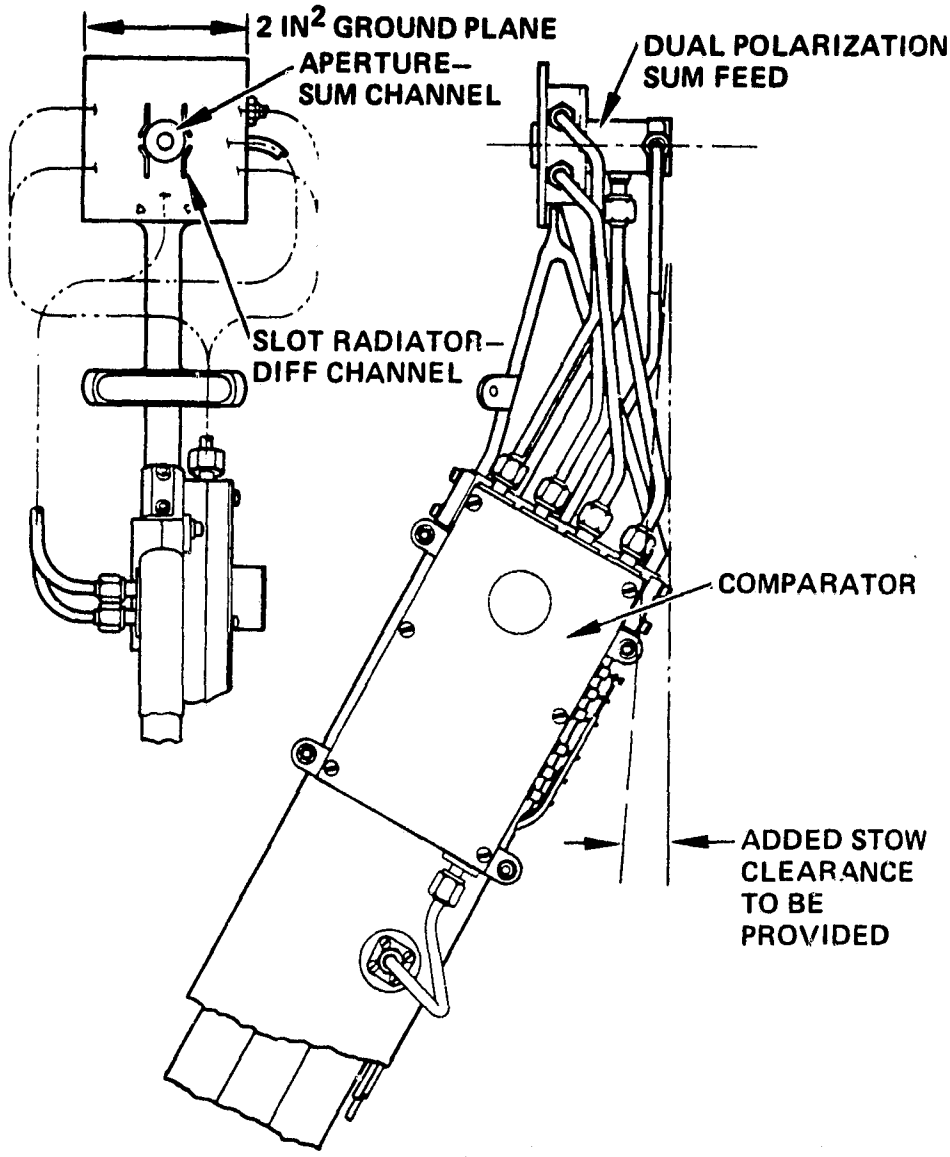

Figure 2. Feed and Feed Support Structure for the Ku-Band Antenna System

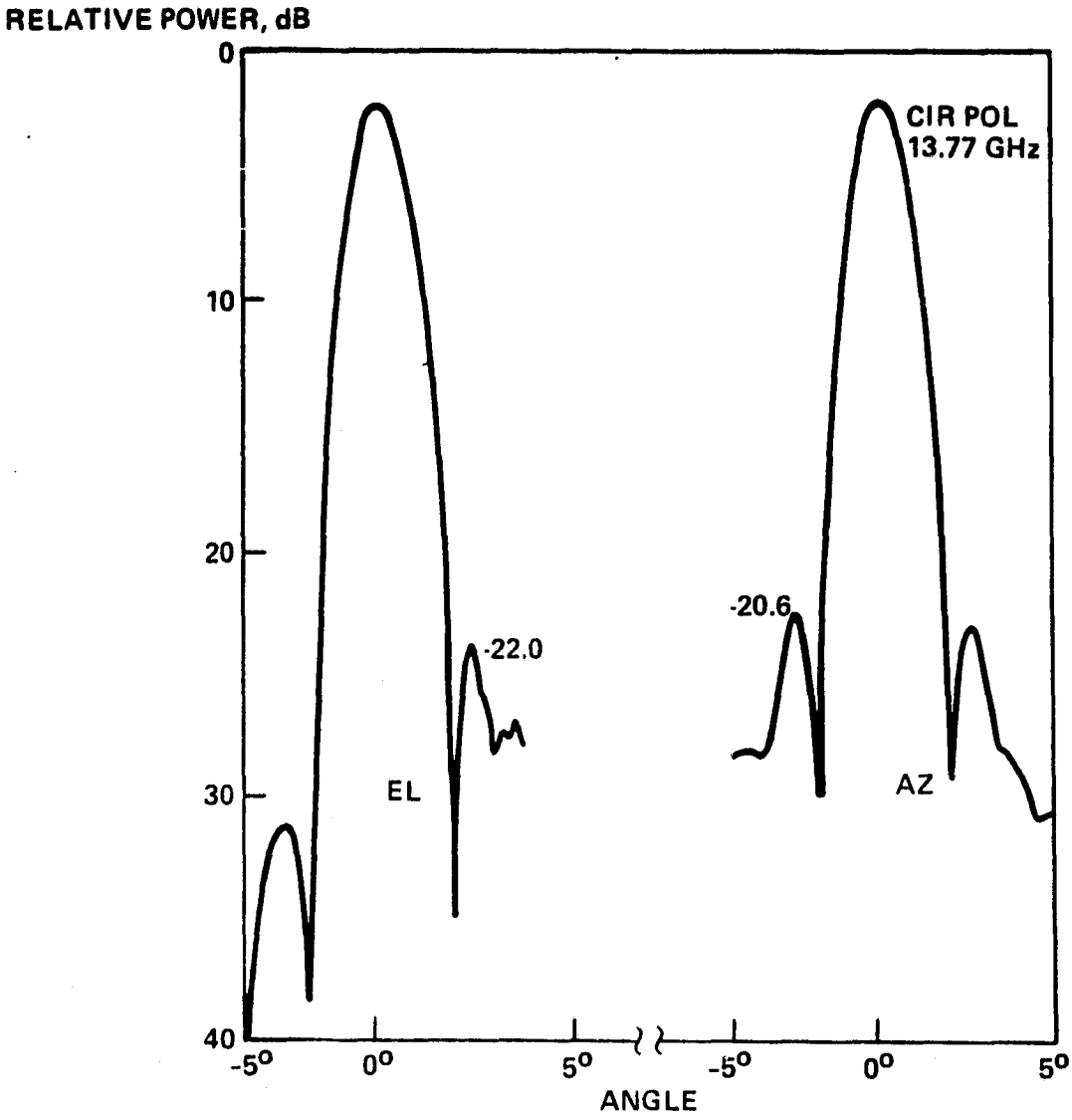

Figure 3. Principal Plane Ku-Band Pattern Measurements for the Circularly Polarized Communication Mode

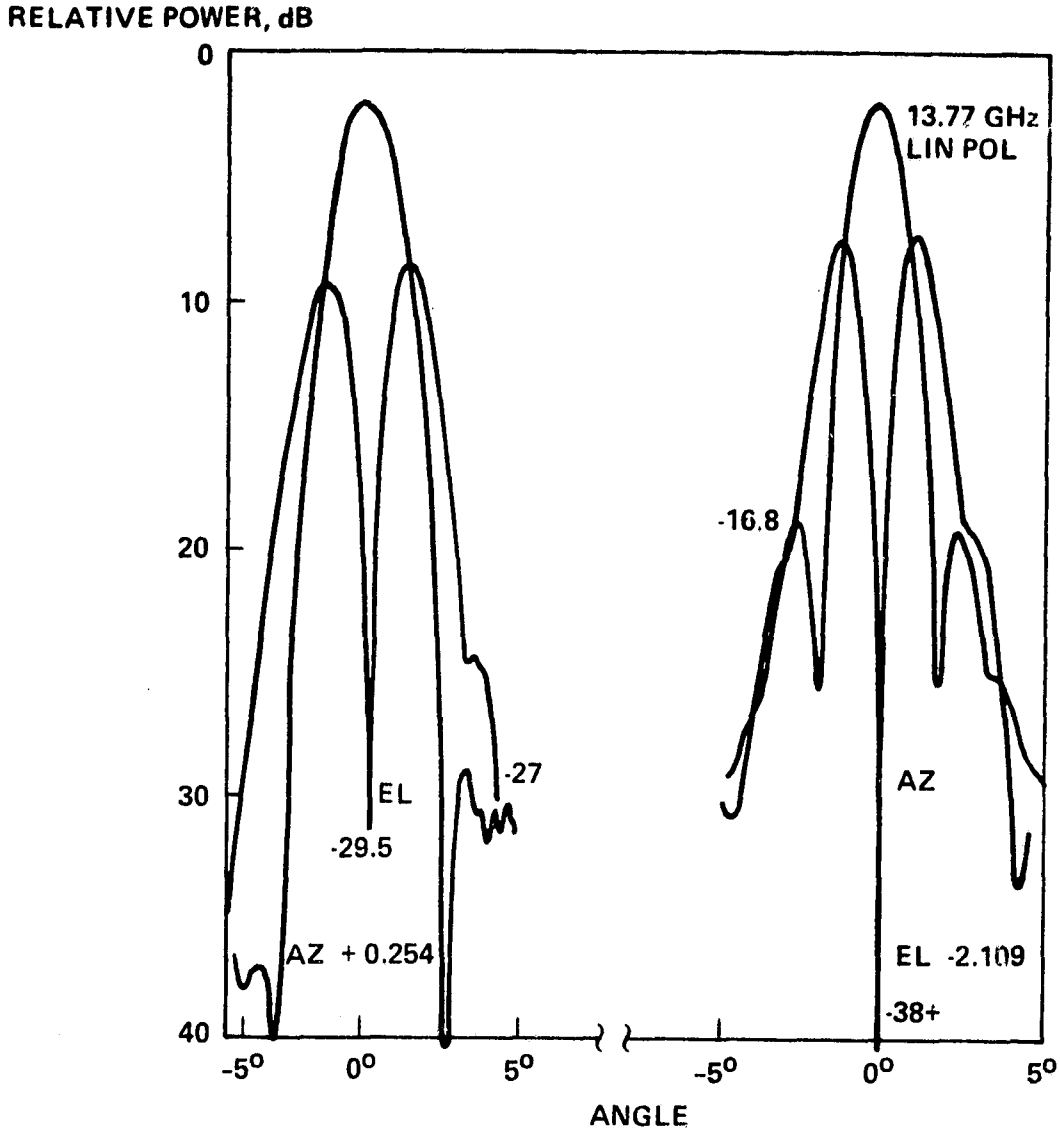

Figure 4. Principal Plane Pattern Measurements for the Sum and Difference Channels of the Ku-Band Antenna for the Linearly Polarized Radar Mode

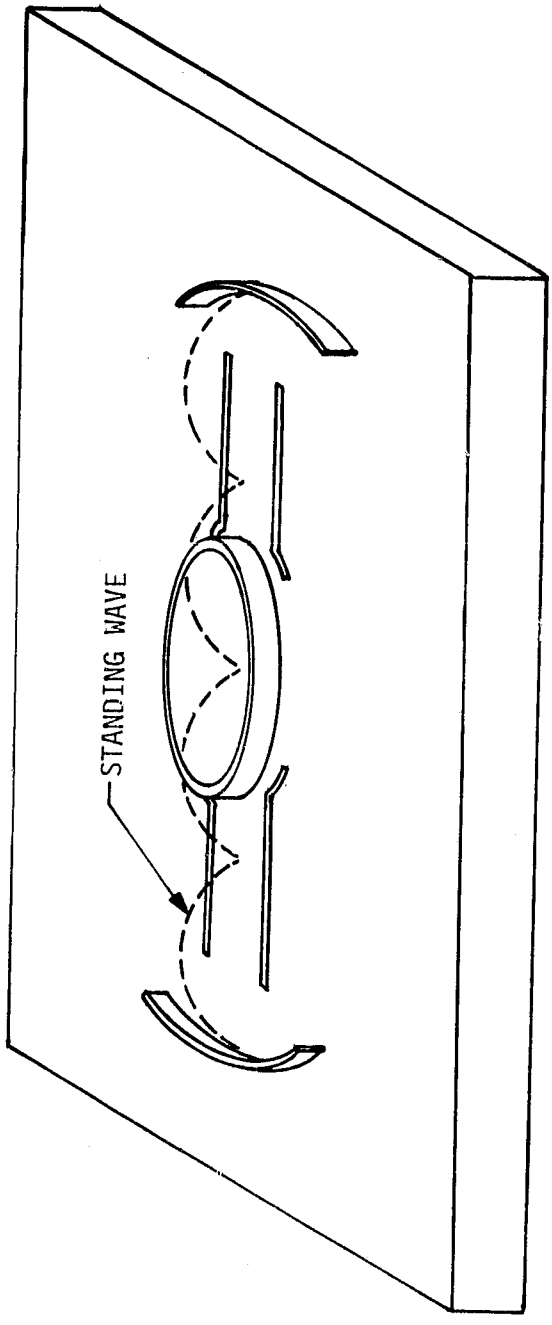

Figure 5. Annular Ring Sector Short to Reduce Mutual Coupling

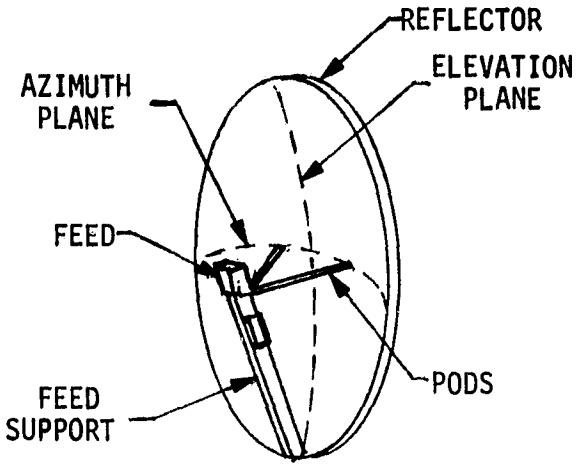

Figure 6a. Sketch of Support Pods on the Ku-Band Antenna

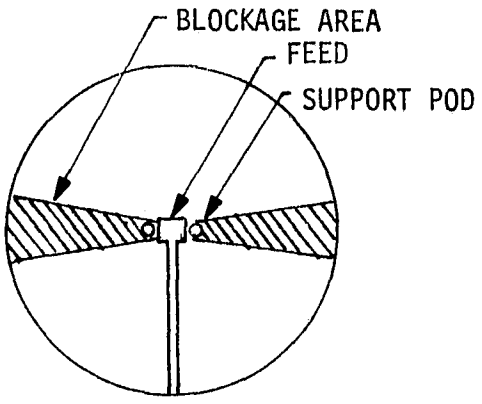

Figure 6b. Obstructed Primary Feed Pattern

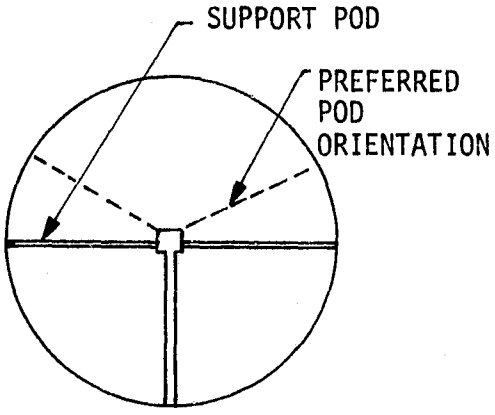

Figure 6c. Reflector Edge Pods

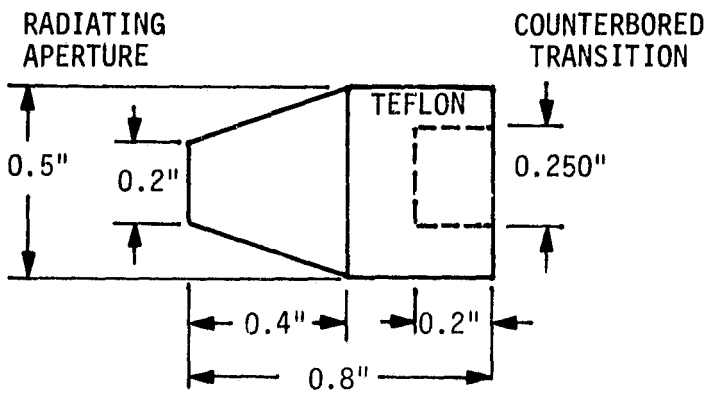

Figure 7a. Present Design of Teflon Plug

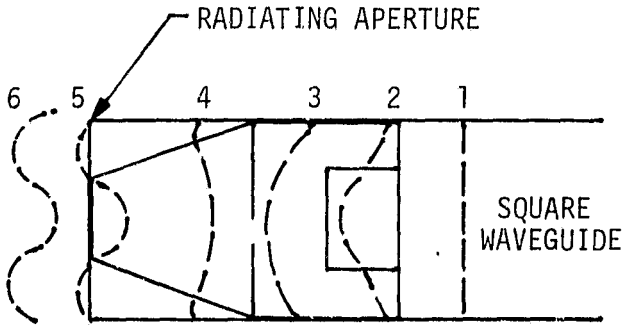

Figure 7b. Sketch of Approximate Phase Fronts for the Present Teflon Plug

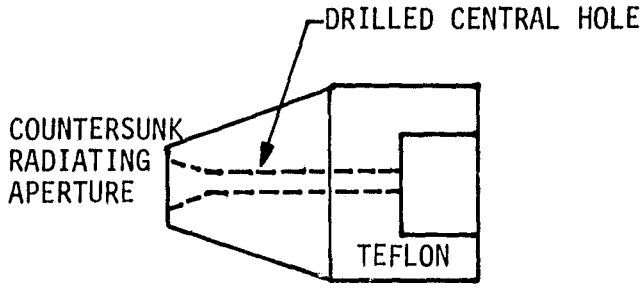

Figure 8a. Modified Design of Teflon Plug to Encourage Quasi-Spherical Wavefront

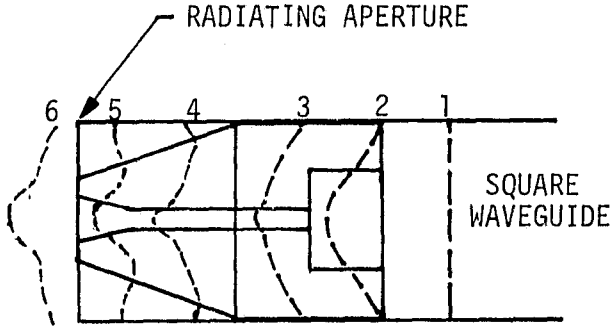

Figure 8b. Sketch of Approximate Phase Fronts for the Modified Teflon Plug

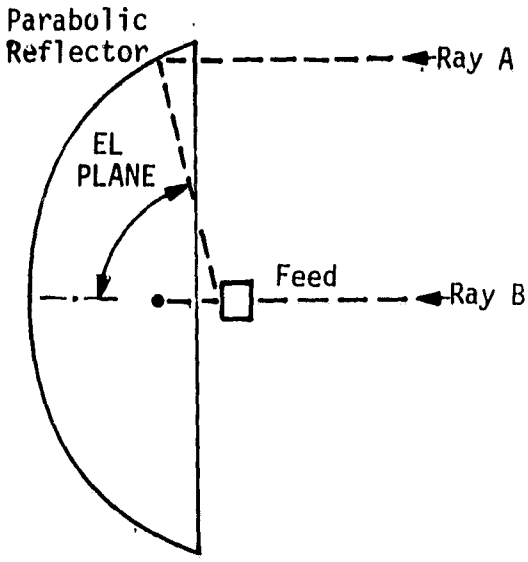

Figure 9a. Ray Paths for the Parabolic Antenna

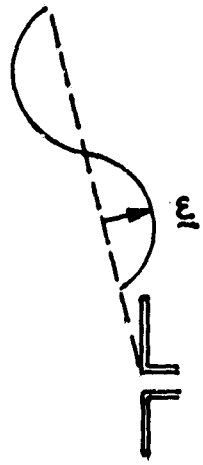

Figure 9b. Incident Electric Field on the Dipole

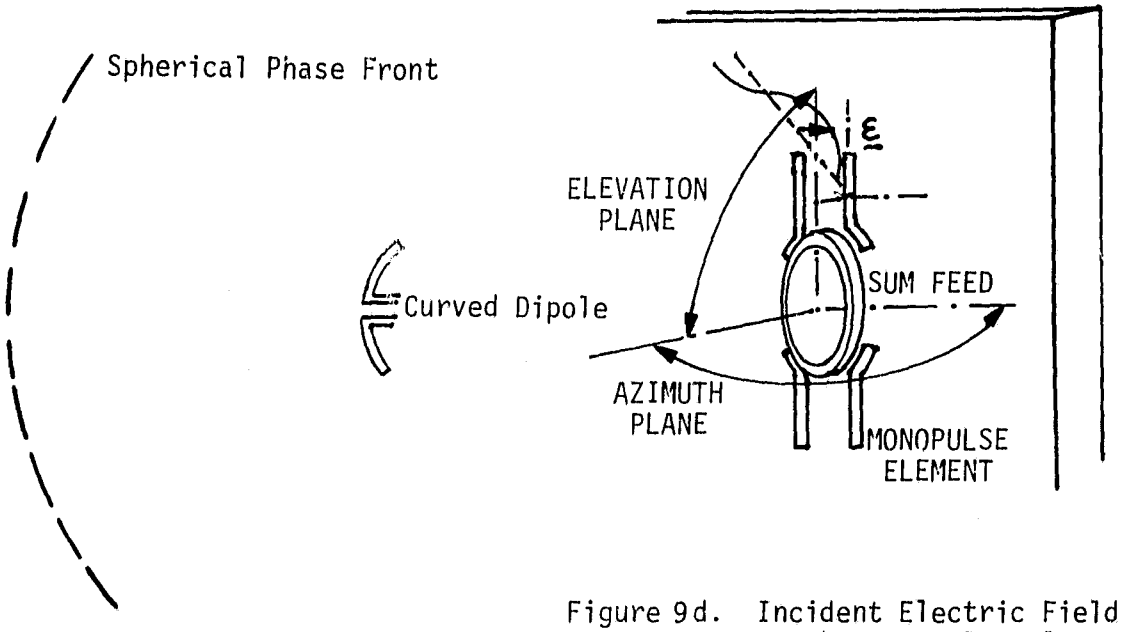

Figure 9c. Curved Dipole Configuration

Figure 9d. Incident Electric Field on the Monopulse Element

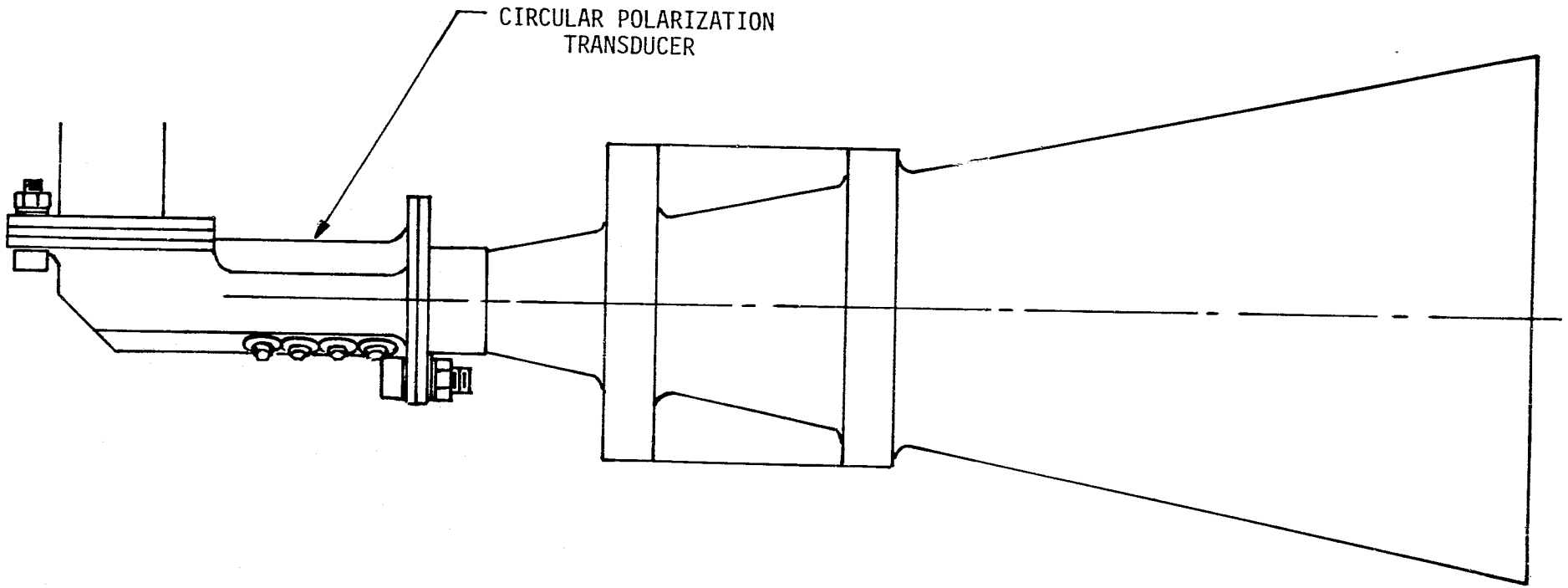

Figure 10. Sketch of Ku-Band Wide Beam Conical Horn with Circular Polarization Transducer

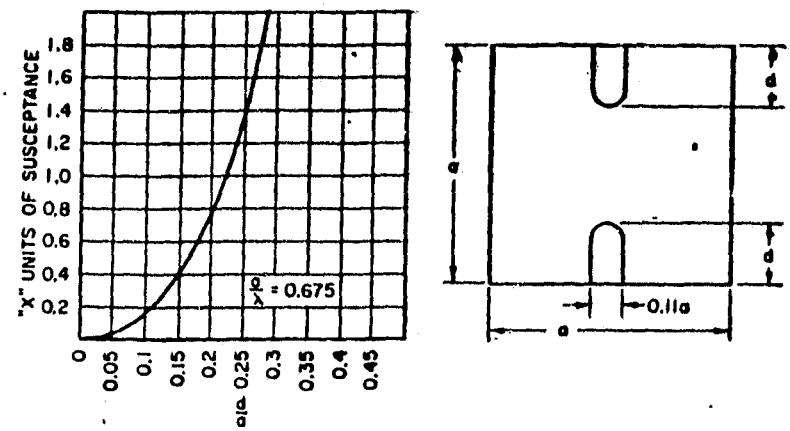

Figure 11a. Susceptance as a Function of Probe Penetration.

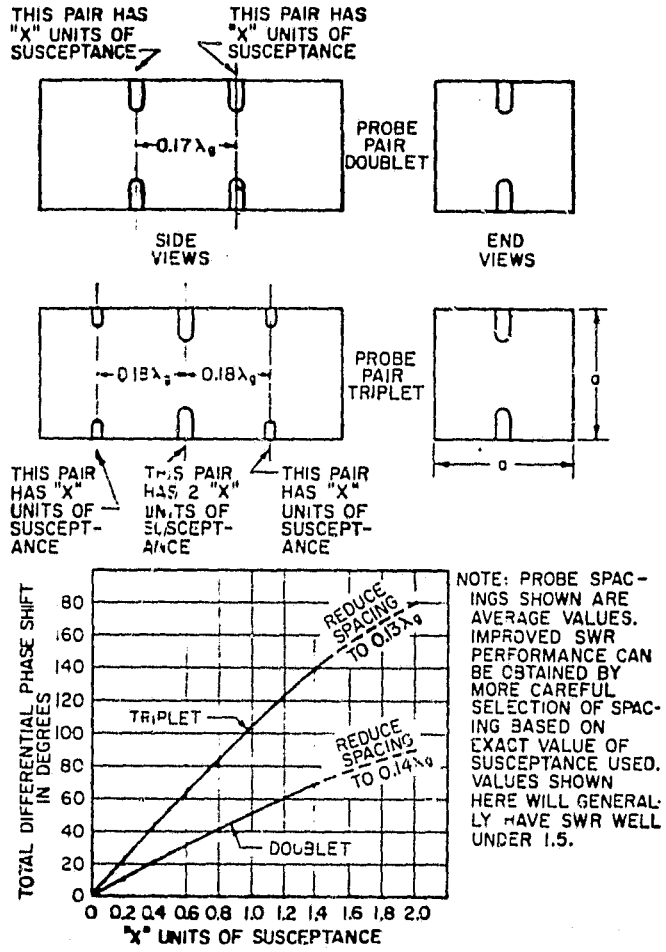

Figure 11b. Probe phase-shifter design.

APPENDIX A

DEGRADATION OF SHUTTLE RADAR PERFORMANCE DUE TO PEJORATIVE ANTENNA SCAN OVERLAP

By

Phyllis Broad

August 1979

1.0 INTRODUCTION

Stability considerations of the deployed assembly (DA) fixed base on the Shuttle may cause the antenna scan overlap to fall below the recommended value for off-zenith-centered scans. A lower antenna scan overlap will cause a lower antenna gain and can lead to shorter target dwell times. This will cause a corresponding decrease in the probability of target detection when the worst-case detection scenario is considered, i.e., detection in the center of the overlap region.

This report will present the relationship between the antenna overlap, dwell time and antenna gain, and their effects on the received target signal-to-noise ratio (SNR) and resulting probabilities of detection.

2.0 TARGET DWELL TIME CONSIDERATIONS

The target dwell time is a function of the total allowed scan time, the scan frequency and the antenna overlap between consecutive scans. The spiral scan geometry is shown in Figure 1, including the antenna overlap region. It should be observed that the overlap region and, consequently, the chord corresponding to the dwell time are defined in terms of the null-to-null beamwidth, θ_n, instead of the half-power beamwidth, θ_B. This has been done to account for the possibility of overlap below the 3 dB point.

Following the procedure outlined in [1], the dwell time, t_d, for a hybrid spiral scan is given by

$$t_d = \frac{T_s \theta_n \theta_0 (1-\Delta) + \theta_0 \sqrt{\left[T_s \theta_n f_s (1-\Delta)\right]^2 - \left[\theta_m - \frac{\theta_n}{2}(1-\Delta)\right]^2}}{2\pi \left[\theta_m - \frac{\theta_n}{2}(1-\Delta)\right]^2} \qquad (1)$$

where T_s = total scan time = 60 sec
θ_n = null-to-null beamwidth = 2.08^o
θ_0 = antenna chord sweeping across the target
Δ = antenna overlap with respect to θ_n
f_s = scan frequency = 2 Hz
θ_m = maximum scan limit = 30^o

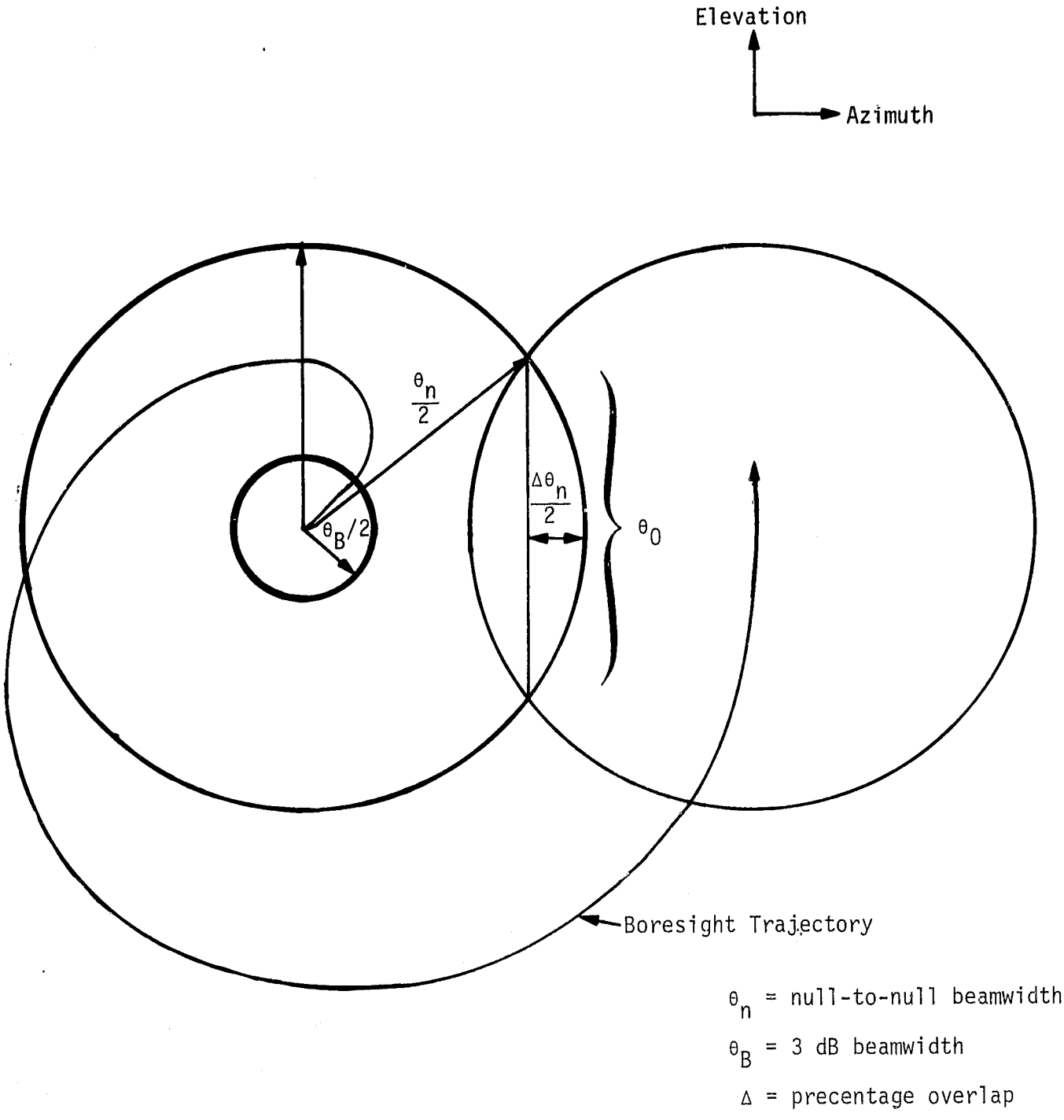

Figure 1. Geometry of Spiral Scan, Including Overlap

A high target dwell time is desirable since it increases the received target energy. However, it should be noted that the dwell time in this case is constrained by the total scan time allowed; too high an antenna overlap precludes completing the volume to be scanned and is physically impossible. A graph of the dwell time is given in Figure 2 as a function of the antenna overlap. As expected, the time on target is equal to zero when no overlap occurs. Maximization of the dwell time, ignoring related effects such as antenna gain, is seen at a scan overlap of 25-30% when measured with respect to the null-to-null beamwidth.

3.0 CALCULATION OF PEAK ANTENNA LOSS

Since the worst-case detection will occur in the center of the overlap region at some point down the antenna mainlobe, a loss must be computed to account for the degraded peak antenna gain illuminating the target. This is not the same as the beamshape loss, which is incurred as the beam sweeps across the target and is included in the system loss budget.

For small values of off-boresight antenna angles and excluding the sidelobes, the antenna mainlobe weighting function may be approximated by

$$W(\theta) = \left[\frac{\sin\left(\frac{\pi\theta}{\theta_B}\right)}{\left(\frac{\pi\theta}{\theta_B}\right)}\right]^2 \qquad (2)$$

where θ = angle off-boresight = $(1-\Delta)\theta_n/2$

θ_B = 3 dB beamwidth = 1.6^o

θ_n = null-to-null beamwidth = 2.08^o

For $\Delta = 1$, corresponding to complete overlap or the on-boresight case, the weighting function is equal to one and the mainlobe is fully weighted. As the scan overlap moves away from the center of the beam, the antenna gain is weighted less. A revised value of the antenna peak can be found as a function of the scan overlap, Δ. A plot of this modified peak gain is given in Figure 3. As noted above, instances when $\Delta = 0.7$ or higher are physically unrealizable and are shown as limiting cases only.

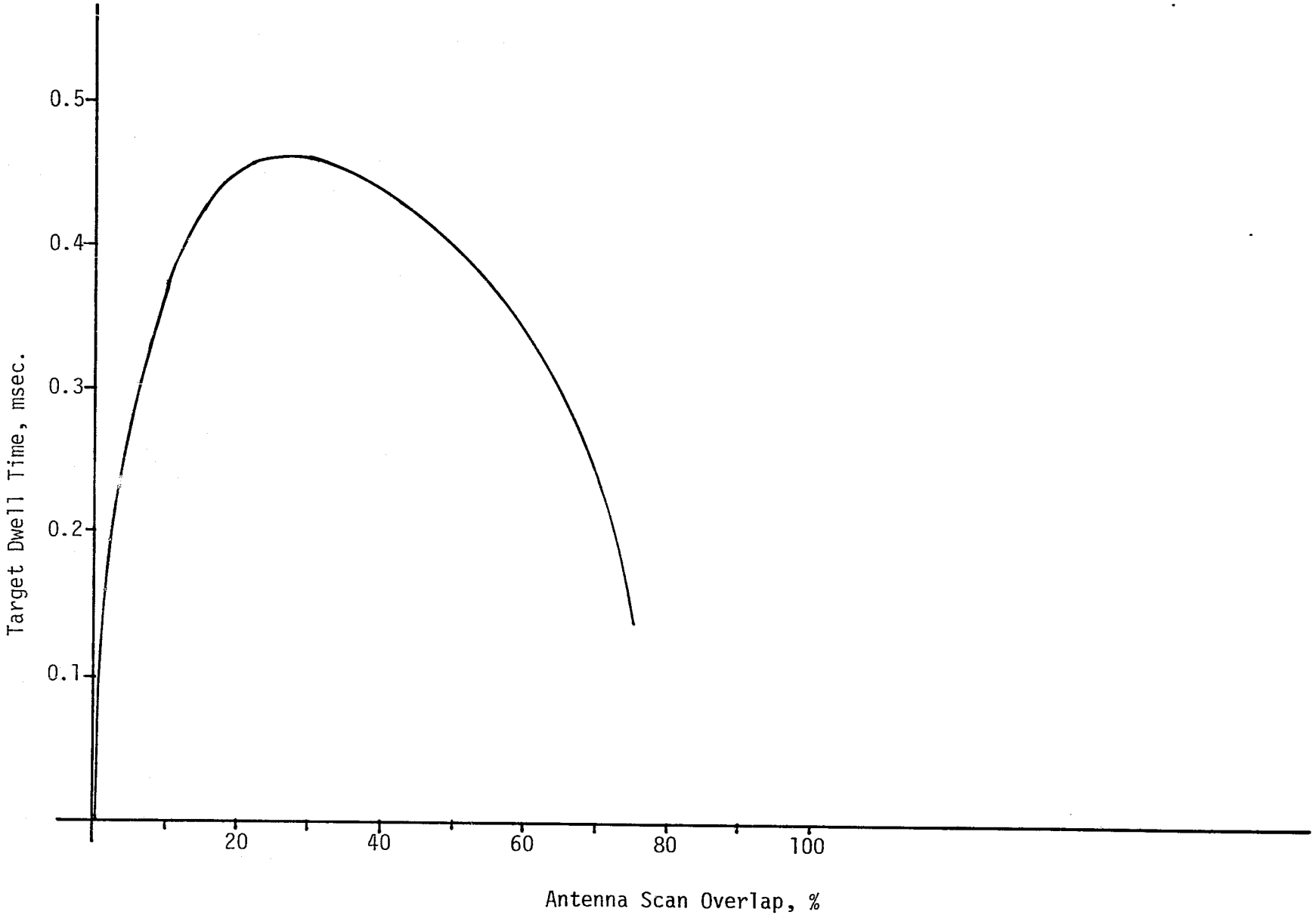

Figure 2. Target Dwell Time as a Function of Antenna Scan Overlap

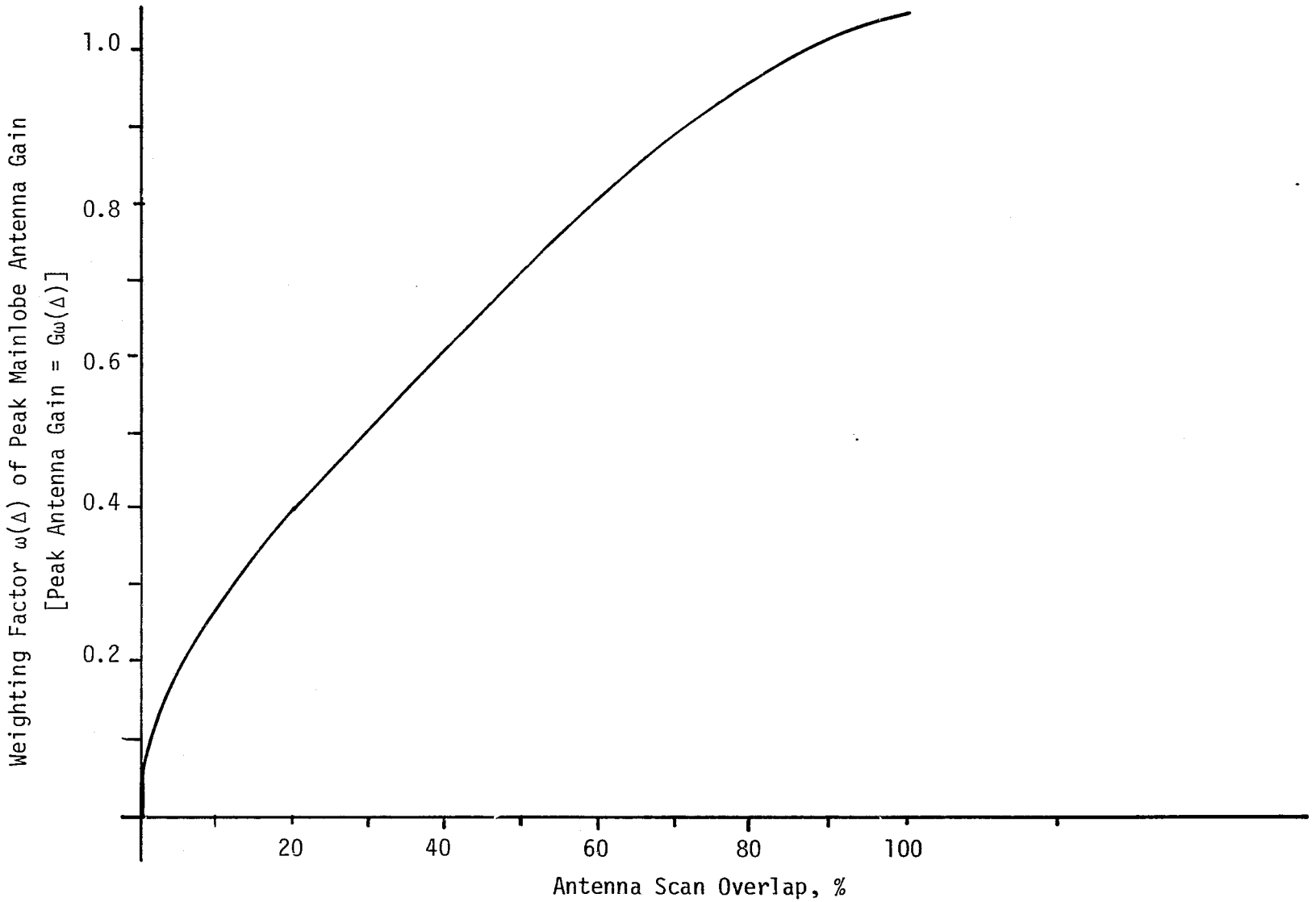

Figure 3. Weighting Factor of Peak Mainlobe Gain as a Function of Scan Overlap

4.0 PULSEWIDTH AND PULSE REPETITION FREQUENCY (PRF)

The pulse duration, τ, of the RF pulse and the PRF are functions of the designated range to target in the Shuttle Ku-band radar. These signal parameters are summarized according to range in Table 1.

Table 1. Radar Pulsewidth and PRF as a Function of Target Range

Range to Target, nmi	τ(μsec)	PRF (Hz)
7.2 +	66.4	2987
3.8 - 7.2	33.2	6970
1.9 - 3.8	16.6	6970
0.95 - 1.9	8.3	6970
0.42 - 0.95	4.15	6970
- 0.42	0.122	6970

5.0 CALCULATION OF AVERAGE SNR

The average SNR, including coherent integration, is found from the radar equation in the following form. The effects of the variable scan overlap are included implicitly via the target dwell time and the peak antenna gain loss, L_B.

$$\overline{SNR} = \frac{P_p \tau \, PRF \, t_d \, G^2 \lambda^2 \bar{\sigma}}{(4\pi)^3 R^4 kT_i LL_B} \tag{3}$$

where P_p = peak transmitter power = 60W

G = antenna gain = 38.5 dB

λ^2 = transmitted wavelength = 0.216 m

$\bar{\sigma}$ = average target cross section = 1 m^2

R = range to target

k = Boltzmann's constant = 1.38×10^{-23} J/°K

T_i = system noise temperature = 1500°K

L = system losses = 13.88 dB

L_B = loss in peak antenna gain

and all other parameters were defined previously.

6.0 PROBABILITY OF TARGET DETECTION

Frequency agility, using five RF frequencies, has been used in both the search and track modes of the radar to minimize target scintillation effects. Therefore, the target is modeled assuming Swerling II scintillation statistics, i.e., a fast fluctuating target. The single-scan probability of detection for this case is given by

$$P_{ss} = 1 - \int_0^{Y_b/(1+\overline{SNR})} \frac{x^{N-1} e^{-x}}{(N-1)!}\, dx \tag{4}$$

$$= 1 - I\left[\frac{Y_b}{\sqrt{N}\,(1+\overline{SNR})}, N-1\right] \tag{5}$$

where Y_b is the receiver bias level, N is the number of pulses integrated noncoherently and $I[\ ]$ refers to the incomplete gamma function.

Radar performance is judged by the probability of detection over two scans. This cumulative probability can be approximated by

$$P_{cum} = 1 - (1 - P_{ss})^2 = 2P_{ss} - P_{ss}^2 \tag{6}$$

if it is assumed that the target range between scans has not changed appreciably. Figure 4 shows the cumulative P_d for different scan overlaps, measured with respect to the antenna 3 dB beamwidth. For example, $\Delta = 0.3$ means that the beam overlap is 30% higher than the half-power beamwidth point, with a probability of detection on one of two scans equal to 0.76 at 10 nmi.

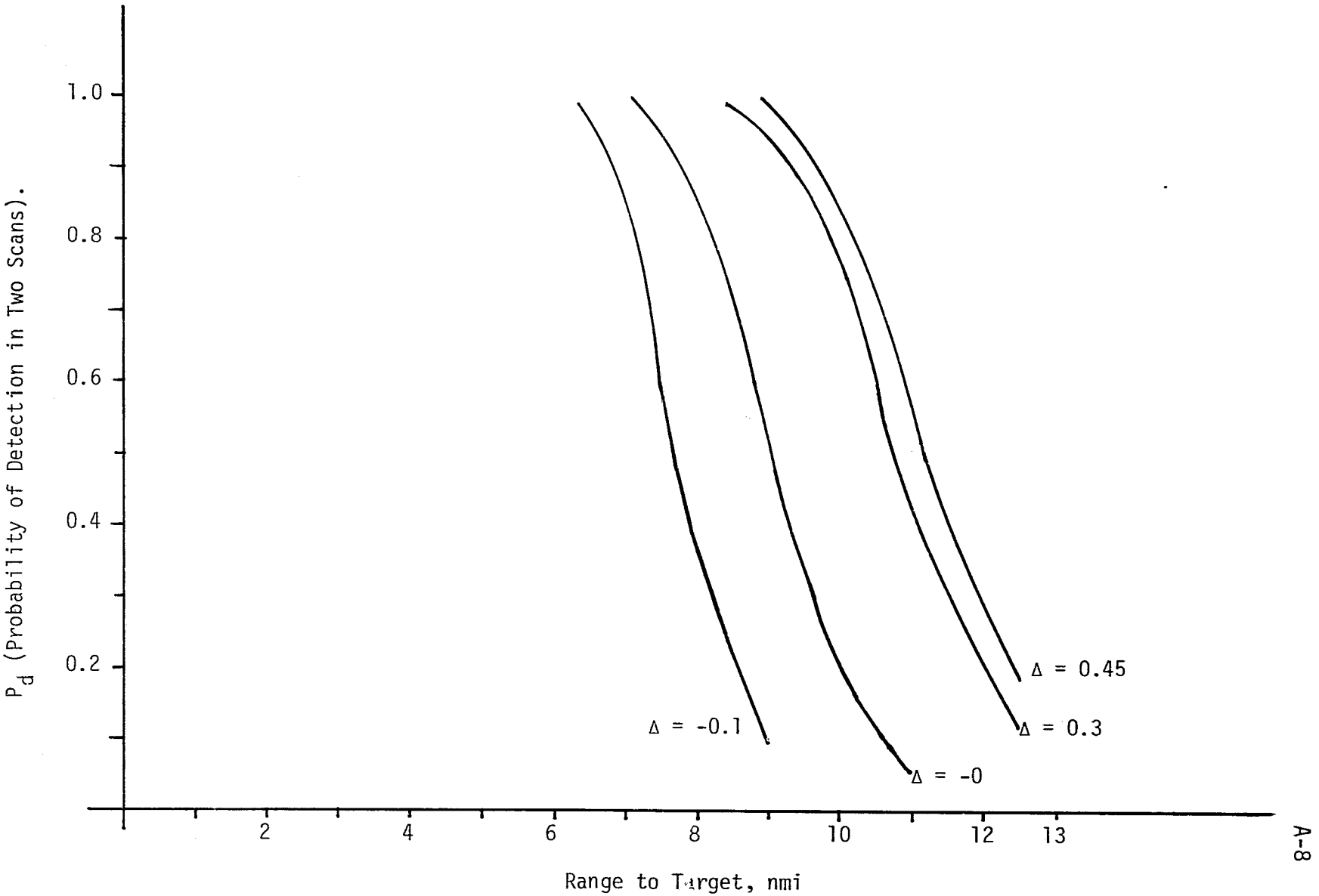

Figure 4. Probability of Target Detection, Servo Bandwidth = 2 Hz.

7.0 CONCLUSIONS

Maximum target energy is received when the antenna scan overlap is approximately 45% when measured with respect to the half-power beamwidth. This compares reasonably with the commonly accepted value of 30% when the approximate nature of the antenna mainlobe model is considered. Probability of detection decreases with lower values of scan overlap until zero detection is "achieved" with no overlap. These results should be considered when deciding which values of scan overlap are tolerable.

REFERENCES

1. Huth, Gaylord K., and Udalov, Sergei, "Spiral Scan Analysis," Axiomatix Report No. R7607-4, July 31, 1976.